Egypt. J. Chem. **Vol. 67**, No. 7 pp. 513 - 524 (2024)

Egyptian Journal of Chemistry

http://ejchem.journals.ekb.eg/

Green Spectrophotometric Assessment for Molnupiravir Quantification in Pharmaceutical Formulations and Biological Fluids: Study of Structural Elucidation and Theoretical Approach

Sabrein H. Mohamed[a,b*], Samir A. Abdel-Latif [c], Aida L. El-Ansary [b], Alyaa I. Salim[d]

[a] *Chemistry Department, College of Science, Jouf University, P. O. Box 2014, Sakaka, Saudi Arabia*

[b] *Chemistry Department, Faculty of Science, Cairo University, 12613, Cairo, Egypt*

[c] *Chemistry Department, Faculty of Science, Helwan University, 11795, Cairo, Egypt*

[d] *Faculty of Biotechnology, Nile University, Giza, 12613, Egypt*

Abstract

The FDA-approved antiviral drug molnupiravir (MPV) was investigated using a green spectrophotometric approach. With the help of mass spectrometry, UV-visible spectroscopy, and Infrared Fourier transform spectroscopy, this drug was characterized and elucidated structurally. This approach depends on measuring the absorbance in doubly distilled water as a solvent at 240 and 285 nm. Variable parameters were estimated and optimized. Beer's law is up to 35.0 µg/mL under optimal conditions with a correlation coefficient (r2)>0.99. Based on this evaluation, the new method was found to be highly sensitive with a LOD and LOQ of 0.34-0.78 and 1.13-2.59 µg/mL, respectively. Analyses provided reproducible results with a 2.0% relative standard deviation (RSD). As a result of the application of the proposed method, MPV levels were successfully achieved in raw materials, pharmaceutical formulations, and biological fluids. The geometry and energy quantum mechanical calculations were also performed using Becke's three-parameter exchange functional method. Using water as a solvent, Lee-Yang-Parr correlation functional analysis (B3LYP/DFT) confirmed the measured results.

Keywords: *Molnupiravir; Spectrophotometry; Molecular geometry; Covid 19*

1. Introduction

Global health leaders face the COVID-19 pandemic (Coronavirus Disease) in the year 2020, the largest public health crisis in a century. The third coronavirus, SARS-CoV-2, was initially identified in December 2019 in China. It is not the only virus with this characteristic; additionally, there are SARS-CoV and MERS-CoV, the Coronaviruses responsible for severe acute respiratory syndromes [1]. Even though the SARS-CoV and MERS-CoV epidemics were mostly contained due to public health efforts, the possibility of future outbreaks emphasizes the importance of safe and effective COVID therapies [2, 3]. There is an increased risk of death associated with COVID-19 in elderly or immunocompromised patients, or those with comorbid conditions such as hypertension, diabetes, malignancies, cardiovascular disease, or chronic lung disease [1, 4].

The need for adequate therapy to overcome this health catastrophe continues to grow [5]. During the worldwide outbreak of Coronavirus disease (COVID-19), most researchers focused their attention on developing treatments that could slow its growth [6].

Fig. 1: Plain structural formula of molnupiravir.

*Corresponding author e-mail: *sabrein@sci.cu.edu.eg*, *sharby@ju.edu.sa*

EJCHEM use only: Received date 28 August 2023; revised date 16 December 2023; accepted date 18 December 2023

DOI: 10.21608/EJCHEM.2023.232340.8515

As well as some expensive and difficult-to-manufacture drugs that require hospitalization to treat COVID-19 like Remdesivir, there are other FDA-approved medicines for this condition [7]. Molnupiravir (MPV) is the most promising, broad-spectrum class for the treatment of COVID-19 [8].

Molnupiravir (MPV), Fig.1; the drug works against severe acute respiratory syndrome coronavirus 2 (SARS-CoV-2), it is an oral, small-molecule antiviral prodrug.

There have been two methods for determining MPV previously published, including an LC-MS/MS method [9, 10] and one RP-HPLC method [11]. As a result, this study is based on the development of a spectrophotometric protocol as a fast, simple, robust, precise, and sensitive strategy for the quantification of MPV in pure form, pharmaceutical formulation, and biological fluids. The proposed method involved the use of water as a diluent which matches green chemistry requirements. The structural elucidation and characterization of MPV were carried out utilizing FTIR, mass spectrometry, and nuclear magnetic resonance (NMR) instruments. Additionally, based on experimental results, MPV was computationally analyzed using density functional theory. A natural bond orbital analysis (NBO) has been used to investigate molecular interactions, intermolecular interactions, and intramolecular interactions. Different calculations were carried out using the DFT-B3LYP/6-11G** level. The calculated quantum chemical parameters are bond angles, bond length, and electronic dipole moments. As a result of DFT analysis, MPV shape, size, vibrations, stability, and reactive areas can be fully explained.

2. Experimental

2.1. Materials and Apparatus

High-grade analytical reagents were used throughout the study. MPV raw material and Molnupiravir® capsules were acquired from Hekma pharmaceutical company, in Egypt.

To obtain spectral measurements in the range of 200-400 nm, a Jenway 61O5 UV/VISIBLE single beam spectrophotometer equipped with quartz cells of 1.0 cm optical path length was used. At Cairo University, Giza, Egypt, the Micro Analytical Center, Faculty of Science, conducted a series of experiments, involving mass spectrometry, FTIR spectroscopy, and nuclear magnetic resonance. A test scan Shimadzu FTIR spectrometer was used to obtain FTIR absorption spectra using the KBr disc technique. On a 300 MHz NMR spectrophotometer, ^{1}H-NMR spectrum was obtained utilizing the deuterium oxide and D_6-DMSO with an internal standard of tetramethyl silane on a Varian 300 MHz NMR spectrometer. Shimadzu (Japan)'s Q 1000 Ex GCMS was used for mass spectrometric measurements at 70 eV and 100 μA.

2.2. *Standard solutions*

To prepare MPV stock solutions, 16.47 mg of solid MPV was dissolved in 50.0 mL double distilled water to prepare 1.0 mmol/L. Solutions covering the range from 100 to 8000 ng/mL were further prepared for constructing the calibration curves.

2.3. *Pharmaceutical preparations*

To prepare Molnupiravir®, ten capsules were weighed, and the average weight was taken from each. This is equivalent to 400.0 mg of MPV, then dissolved in double distilled water. Filtering the prepared solution and washing the excipients with the same solvent ensured that the main active ingredient was completely dissolved. Upon using double distilled water, the solution was then completed to 50.0 mL.

2.4. *Investigation of serum and urine synthetic samples*

In preparing the spiked samples, diverse volumes of 10.0 mmol/L MPV solution covering the range from 0.1 to 100.0 nmol/mL were added to urine and serum samples. After mixing well, the latter was added to doubly distilled water and completed to 10 mL using double distilled water. Utilizing the standard addition strategy, these solutions were measured as illustrated above.

2.5. *Computational details*

MPV's molecular conformation was determined by performing an energy minimization analysis with Gaussian-09W software [12]. A geometrical optimization of the ground state was performed using DFT and B3LYP exchange-correlation functionals [13, 14]. Carbon, hydrogen, nitrogen, and oxygen atoms were subjected to a basis set 6-311G [15]. A symmetry-free solution phase optimization was achieved. A molecular orbital diagram was created utilizing software (Gauss view, 5) [16]. The following equations were used to calculate the quantum chemical parameters; E(LUMO), E(HOMO), η (absolute hardness), Eg (Energy gap), (chemical potential), ω (global electrophilicity), χ (absolute electronegativity), electronic charges, S (global softness), and ΔNmax.[17, 18].

$E_g = E_{LUMO} - E_{HOMO}$

$\chi = E_{LUMO} - E_{HOMO}/2$

$\eta = E_{LUMO} - E_{HOMO}/2$

$\pi = -\chi$

$S = {}^{1}/_{2}\,\eta \qquad \omega = \pi^2/2\eta$

$\Delta N_{max} = -{}^{\pi}/_{\eta}$

3. Results and Discussion

3.1. Molecular orbital treatment

The level of the theory DFT-B3LYP/6-311G** was utilized to make a study for the spectral characteristics and the electronic structure of MPV. The geometry of MPV should be characterized before making the calculation of the electronic structures utilizing a harmonic frequency analysis. Figure 2 shows the numbering of atoms and the optimized geometry of MPV. Table 1 shows the selected angles and bond distances. It is concluded that MPV is not present in the same plane (non-planar) due to the dihedral angle values of it being far from 0º or 180º. The geometrical structure was optimized by DFT-B3LYP/6-311G** level, Table 1.

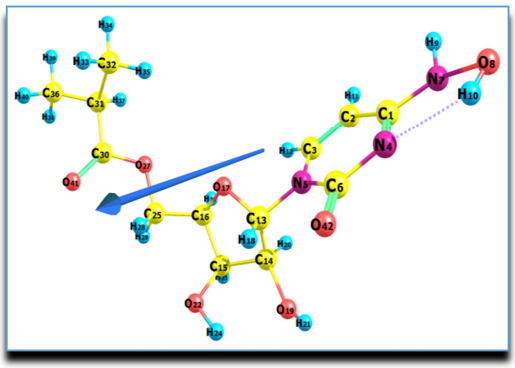

Fig. 2: B3LYP/6-311G** Optimizations level for numbering system, geometry, and dipole moment vector.

3.1.1. Descriptors of global reactivity and ground state properties

HOMO and LUMO energy parameters are depending on chemical reactivity, kinetic/thermodynamic stability, and charge transfer.

HOMO and LUMO orbitals can be used as predictors of the most reactive positions in conjugated systems [19].

At 4.9718 eV, MPV has a difference in energy between its HOMO and LUMO states. MPV can easily polarize due to increased reactivity because of electron transfer between HOMO and LUMO energies.

Calculations of η (Chemical hardness), χ (electronegativity), Π (chemical potential), and S (global softness) were done in Table 2. Lower values of η and S mean that there is no probability of charge transfer and MPV has a lower chemical hardness. From Table 2, the electron affinity value is 1.4523 eV, and LUMO and HOMO energy values were -0.0534, and -0.2361, respectively with E_g of 4.9718 eV indicating the stability of the molecule. From the results, it can be concluded that HOMO is in a six-membered ring and partially found in a five-membered ring. Whereas LUMO is located over the six-membered ring, Fig. 3.

Table 1: B3LYP/6-311G** level for the optimized MPV selected geometric bond length, dihedral angle, and bond angles

Bond Length, Å		Bond Angle		Dihedral angle	
C 1- C 2	1.43	C1-C2-C3	115.42	C 1- C 2-C 3- N 5	-0.501
C 2- C 3	1.36	C2-C3-N5	121.74	C2-C3-N5-C6	3.435
C 3- N5	1.36	C3-N5-C6	121.55	C3-N5-C6-O42	175.900
N5-C6	1.44	N5-C6-N4	115.74	N5-C6-N4-C1	1.775
C6-N4	1.37	C6-N4-C1	121.32	C6-N4-C1-C2	1.095
C6-O42	1.21	N4-C6-O42	124.52	C6-N4-C1-N7	-176.497
C1-N4	1.32	C1-N4-C6	28.68	N4-C1-N7-O8	-12.368
C6-O42	1.21	C1-N7-O8	116.42	N4-C1-C2-C3	-1.833
C1-N7	1.36	C2-C1-N7	120.18	C3-N5-C6-N4	-4.033
N7-O8	1.40	C28-C31-C35	109.19	C1-N4-C6-O42	-178.154
N4-H10*	1.92	N7-O8-H10	101.22	N5- C13-O17-C16	144.059
N5-C13	1.46	N5-C13-O17	109.19	N5- C13-C14 -C15	-155.747
C13-C14	1.54	C13-C14-O19	110.19	C13-C14 - C15-C16	36.685
C14-C15	1.54	C14-C15-O22	109.60	C13-C14 - C15-O22	-80.215
C15-C16	1.53	C15-C16-O17	106.39	C14-C15-C16-C25	-147.455
C16-C25	1.51	C16-C25-O27	106.64	C15-C16-C25-O27	-172.671
C15-O22	1.42	C25-O27-C30	116.30	C16-C25-O27-C30	-173.010
C14-O19	1.42	O27-C30-O41	123.18	C25-O27-C30-C31	174.750
C25-O27	1.44	O27-C30-C31	110.69	O27-C30-C31-C32	-70.898
O27-C30	1.36	C30-C31-C32	109.28	C30-C31-C32-C36	164.755
C30-O41	1.21	C30-C31-C36	110.98		
C30-C31	1.52				
C31-C32	1.54				
C31-C36	1.53				

Table 2: Quantum chemical parameters of MPV by DFT-B3LYP/6-311G** level

Geometrical Parameter	Value
Et	-1197.922 a.u.
E_{HOMO}	-0.2361 a.u.
E_{LUMO}	-0.0534 a.u.
I, ionization potential, for E_{HOMO}	6.4241 eV
A, electron affinity, for E_{LUMO}	1.4523 eV
E_{HOMO}-E_{LUMO}, E_g	4.9718 eV
X	3.9382 eV
H	2.4859 eV
S	0.2011 eV
π	-3.9382 eV
Ω	3.1195 eV
ΔN_{max}	1.5842 eV

η (Chemical hardness), π (chemical potential), ω (electrophlicity index), χ (electronegativity), S (global softness), and ΔN_{max} (maximum charge transfer.

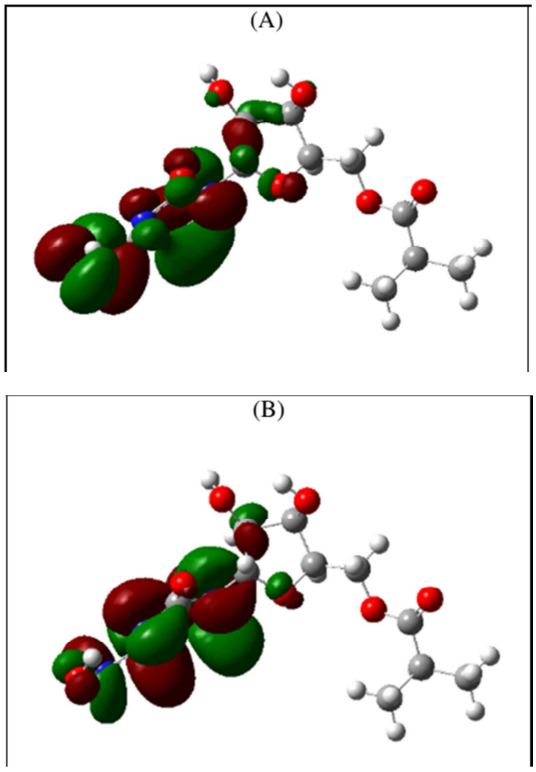

Fig. 3: HOMO, A, and LUMO, B, MPV charge density map by DFT-B3LYP/6311G** level

It has been reported by DC Lee et al. that MPV in plasma is converted into EIDD-1931 (pseudo-cyclic pyranosyl pyrolidinoalkyl monooxycytidine) by the host's esterase. This was confirmed by calculating the energies of MPV and NHC. From Table 2, the total energy of MPV is -1197.922 au. The total energy of NHC is calculated using B3LYP/6-311G** level which was found to be -966.57 au. It is evident from these values that NHC has a higher level of activity than MPV. Many RNA viruses can be inhibited by this NHC [20, 21]. As EIDD-1931 transitions from its inactive form to its active form in host cells, it acts as an inhibitor of viral replication, Fig. 4, [21–23].

3.1.2. Electrostatic potential (MEP) of molecules

It is possible to observe electrophilic effects and nucleophilic effects at the active sites of a studied compound, as well as hydrogen bonding [24]. An increasing potential in the molecule is indicated by red, orange, yellow, green, and blue [25, 26]. Upon using DFT-B3LYP/6-311G** level, the optimized 3D MEP map of MPV is analyzed, Fig. 5. According to the result, the lone-pair electrons from the O27 and O4 atoms explain most of the negative region (red). Meanwhile, hydrogen and carbon are sites with positive (blue) potential. There is no potential value for other carbon atoms. An electrophilic attack is likely to occur on molecules with a negative electrostatic potential. An electrophilic attack is more likely when the potential is negative

3.1.3. NLO, nonlinear optical properties

In the NLO study urea is used as a standard pattern. MPV moment vectors are also determined by the distribution of atomic charges within complexes. A similar calculation level was used to determine mean anisotropy of the polarizability, polarizability, first-order hyperpolarizability, and dipole moment, for MPV as well as urea [27], Table 3. MPV dipole moment is 7.9628 D in the solution phase. The consequences are calculated in esu units utilizing the adaptation factor (0.1482 x $^{10-24}$ esu for α and 8.6393 x 10^{-33} for β). The NLO system emphasizes β value as one of its proper aspects. MPV polarizability value is 6.1092x10^{-24} esu. Based on theoretical calculations, MPV is 6 times greater than urea. A comparison of the studied MPV with urea as a reference substance indicates that it has polarizability and first-order hyperpolarizability properties that indicate it can be considered as a viable candidate for NLO materials.

3.1.4. Studying of TD-DFT Calculation

It was done at the same DFT-B3LYP/6-311G** level to show the origin of the electronic spectrum. The PCM method (polarizable continuum

solvation method) is used to clarify the origin of electronic spectra. In comparison to the solute, water (solvent part) has no structure, whereas the dielectric constant and other parameters show how it behaves on a macroscopic level. The molecular structure of MPV was represented using DT-DFT calculations. When both molecular orbitals are occupied and unoccupied on the same component, the transition is an internal transition [28, 29]. Results show two bands (286 and 250 nm) that characterize the theoretical spectra of MPV which represent $HOMO \rightarrow LUMO$ *and* $HOMO - 1 \rightarrow LUMO$ in this order. HOMO → LUMO is represented at 286 nm with 68.9 percent contribution from $HOMO \rightarrow LUMO\ n - \pi^*$ transition, while the other excitation band (250 nm) is due to 65 percent contribution, $HOMO - 1 \rightarrow LUMO\ \pi - \pi^*$ transition. The allowable transition states are S0→ $S1$ and S0→ $S2$ with effective oscillator strengths of = 0.1187 and 0.2377, respectively in water. FMOs and MPV electron density transfers, which participate in electronic transitions, are described in Figure 6. These obtained results are confirmed experimentally as given below in spectrophotometric study.

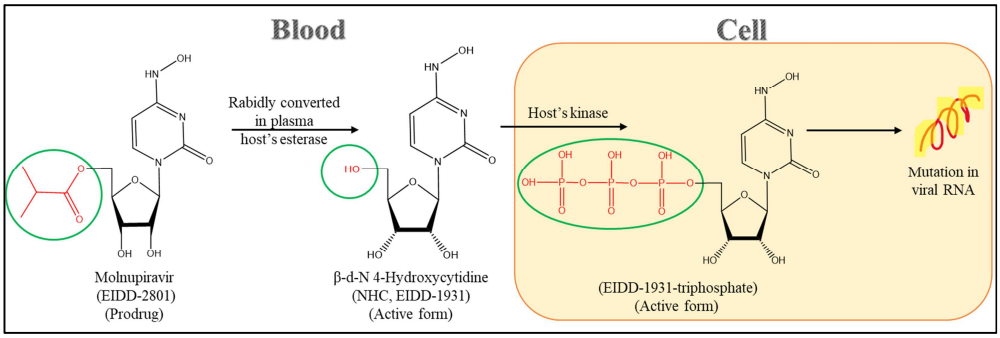

Fig. 4: Mechanism of molnupiravir and its pharmacologically active form after oral administration.

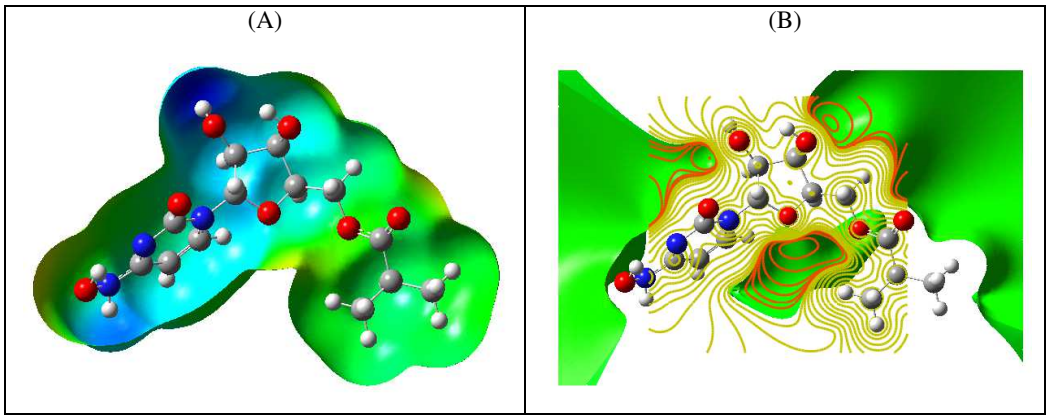

Fig. 5: B3LYP/6-311G** level of MPV surface molecular electrostatic potential, A and contours electrostatic potential, B.

3.2. MPV structural formula investigation

A variety of methods were used to analyze and investigate the drug under investigation, including FTIR, ^{1}H NMR, UV-VIS spectroscopy, and mass spectrometry.

3.2.1. Fourier transforms infrared absorption spectra (FTIR).

In organic chemistry, FTIR is a versatile tool for characterizing the surface properties of particles and identifying functional groups and molecular structures [30]. Experimental one; FTIR spectra of MPV can be seen in Fig. 7 using KBr disc and simulated. Experimental and theoretical bands match each other, as shown in Table 4.

3.2.2. ^{1}H-NMR analysis

As a quantitative and qualitative analytical tool, NMR can be used in a variety of applications in analytical chemistry [30, 31]. Using ^{1}H-NMR, we can determine the number and types of situations in the molecule, as well as the atoms in neighboring groups. An understanding of the structure of the studied drug

was obtained by analyzing 1H-NMR spectroscopy, Fig 8. Table 5 shows the results of the ^{1}H-NMR experiments in DMSO.

Table 3: Calculations of nonlinear optical properties of MPV utilizing B3LYP/6-311G** level using urea as a reference material

Property	Urea	MPV
μ, D	1.3197	7.9628
xx	-	-162.9337
yy	-	-115.624
zz	-	-134.732
xy	-	-6.739
xz	-	9.4586
yz	-	-5.035
<α>	-	-2.0417×10^{-23} esu
Δα	-	6.1092×10^{-24} esu
xxx	-	46.9166
xxy	-	-27.266
xyy	-	-34.14
yyy	-	50.734
xxz	-	-88.0908
xyz	-	-16.5623
yyz	-	-37.2642
xzz	-	-4.0388
yzz	-	-0.3357
zzz	-	-13.9779
<β>	0.1947×10^{-30}	1.2226×10^{-30} esu

Table 4: Experimental and simulated band assignments of FTIR bands for MPV

Assignment	Wave number (cm^{-1})
O-H	3499 (3484)*, 3373 (3221)*, 3298.64
N-H	3125 (3115)*, 2972 (2993)*
C-H Bending	1383 (1380)*, 1347 (1345)*
C=O aliphatic	1736 (1787)*
*Simulated values.	

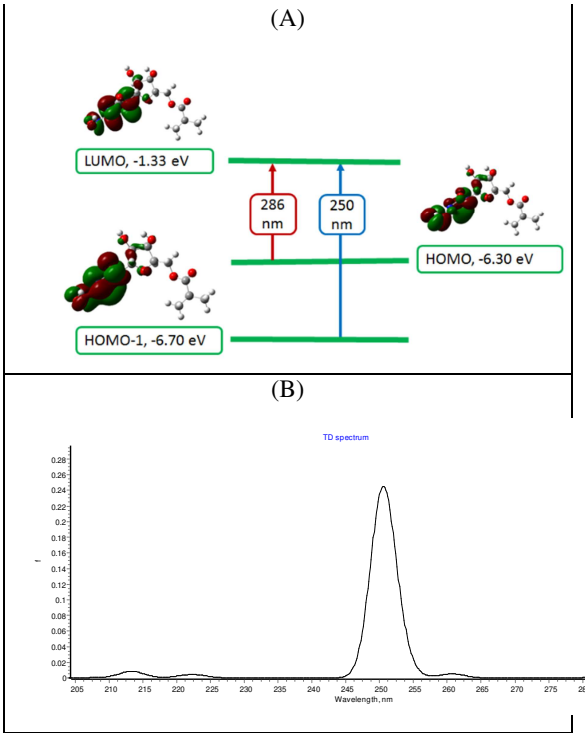

Fig. 6: (A) Frontier molecular orbitals and (B) Calculated TD spectrum involved in MPV's electronic absorption transitions using TD-B3LYP/6-311G** level.

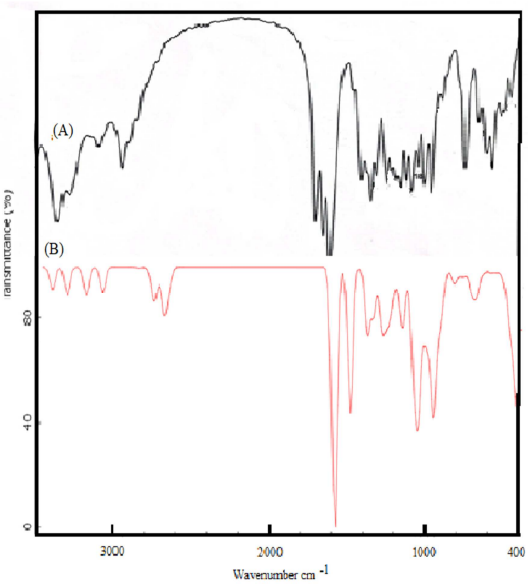

Fig. 7: Experimental (A) and simulated (B) FTIR spectra

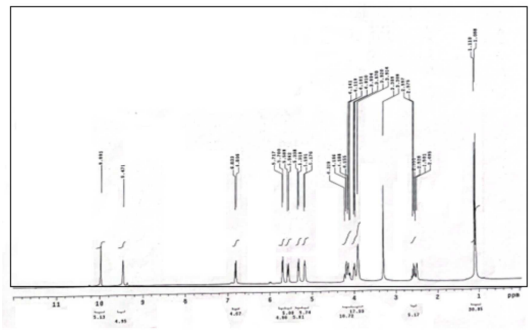

Fig. 8: ^{1}H-NMR spectra of MPV in dimethyl sulfoxide (DMSO).

Based on the analysis of MPV ^{1}H NMR spectrums, Fig. 8, a singlet signal was found at 9.991 ppm can be attributed to three ionizable protons attached to O8, O19, and O22. This signal disappeared after deuteration confirming their ionizable properties. A singlet signal appeared in 1HNMR spectrum of the MPV at 9.471 ppm assignable to one proton of the N7 and disappeared in the deuterated NMR spectrum after deuteration. In addition, doublet signals appeared at 6.8 ppm in 1H NMR spectrum due to C2 and C3 in the aromatic ring. Four doublet signals appeared at 5.17 and 5.71 ppm which may be assignable to the protons attached to C13, C14, C15, and C16 of the five-membered ring. A 4.22 ppm multiplet signal can be attributed to the CH proton of the isopropyl group. A singlet signal at 1.11 ppm, attributed to the proton of the methyl groups, can be seen in the MPV's ^{1}H NMR spectra.

Table 5: Analysis of Molnupiravir ^{1}H NMR spectrum

Assignments	δ, Chemical shifts, ppm
3H/OH	9.991(s)
1H/NH	9.471(s)
4H/aromatic ring	6.8(d)
4H/CH	5.17-5.71
1H/CH	4.22(m)
6H/2CH_3	1.11(s)

(s): singlet, (m): multiplet, (d) doublet.

3.2.3. Mass spectrometric analysis

It is an analytical technique that isolates and distinguishes a mixture of gaseous ions based on their mass/charge (m/z) ratios. To estimate the ion m/z, use M or (M^{+1}), where M is the ion's molecular weight. To evaluate MPV's structure and elemental composition, mass spectrometric analysis was done. The spectra show a molecular ion peak at 329.31.

3.3. UV spectrophotometric methods

3.3.1. Wavelengths selection

In various solvents, the MPV absorption spectra were obtained. Doubly distilled water was chosen as a solvent because it has beneficial spectral characteristics as well as economic and environmental advantages, such as simplicity of procurement and disposal and low cost. The absorbance was calculated using double distilled water as a blank and was measured between 200 and 400 nm. All measurements were made at a temperature of 25°C. At 240 and 285 nm, the maximum absorption was seen (Fig. 9). At 240 nm, the aromatic ring undergoes Π - Π * transition, whereas the band at 285 nm results from an n- Π * transition that is driven by charge transfer throughout the entire molecule [32].

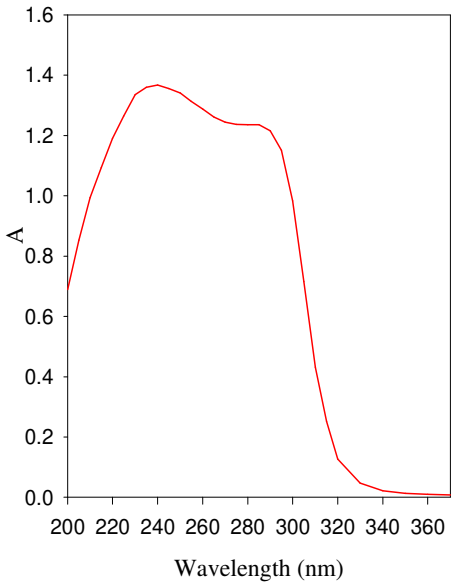

Fig. 9: MPV solution's UV absorption spectrum

3.3.2. Quantification of MPV

3.3.2.1. Direct tool

Laboratory-proposed techniques were validated throughout the investigation to guarantee their quality. The International Conference on Harmonization (ICH) Q2 (R1) recommendations was utilized to validate the laboratory's given methodologies [33]. Calibration curves for MPV were created at the chosen max; 240 and 285 nm under the given procedure conditions, as shown in Fig. 10. Based on RDC 166 (2017) [34], the linear range is up to 35.0 µg/mL with a correlation coefficient (r^2) > 0.99, indicating a linear correlation between absorbance and concentration. The ideal concentration range for Ringbom is 4.68–27.41 µg/mL. At 240 and 285 nm, respectively, the molar absorptivity and Sandel sensitivity are $0.88x10^4$, $0.39x10^4$ L mol^{-1} cm^{-1} and 0.037, 0.085 µg cm^{-2}. This

approach has a wide range of applications, as shown by Table 6.

A method reproducibility was determined by five replicates using 13.172 µg/mL of MPV. The Relative standard deviation (RSD%); <0.40, proves that the techniques proposed are precise.

For the validation, detection, and quantification limits were established [35] based on the following:

$LOD = 3\,^{S}/_{m}$ $LOQ = 10\,^{S}/_{m}$

Where the calibration curve slope is given by m and s is the standard deviation of the blank.

The newly proposed method's great sensitivity was demonstrated by estimates of LOD and LOQ of 0.34-0.78 and 1.13-2.59 µg/mL, respectively.

The equation of least squares was used to evaluate the linearity. By using the least squares method, the typical linear equation was calculated as follows:

Y_{240} =0.027x +0.022 (n = 3); r^2 = 0.9976.

Y_{285} =0.0118x +0.014 (n = 3); r^2 = 0.9968).

In this equation, the MPV solution concentration (in µg/mL) is represented by x, the absorbance value (y), and the correlation coefficient (r^2).

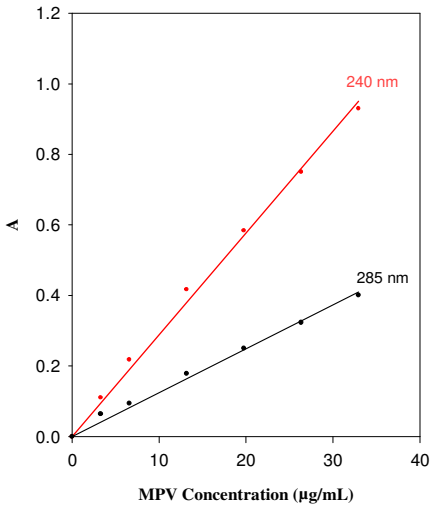

Fig. 10: Validity of Beer's law for MPV at 240 and 285 nm in doubly distilled water.

Table 6: Analytical criteria for quantifying MPV

Parameter	λ max	
	240 nm	285 nm
Beer's law	Up to 35.0 µg/mL	Up to 30.0 µg/mL
Ringbom range, µg/mL	4.68-27.41	5.02-30.32
Sandel sensitivity, µg/cm^2	0.037	0.085
Molar absorptivity (ε), L/mol.cm	0.88x10^4	0.39 x10^4
Intercept	0.022	0.014
Slope, mL/µg.cm	0.027	0.0118
r^2	0.9976	0.9968
Relative standard deviation (RSD%) (n = 5)	0.40	0.33
LOD, µg/mL	0.34	0.78
LOQ, µg/mL	1.13	2.59

3.3.2.2. Standard addition method

A standard addition tool was applied for the raw material and dosage form to eliminate matrix interference and differentiate and distinguish the small concentrations. Using the suggested method, several synthetic solutions with varying concentrations of MPV can be quantified at 240 and 285 nm. In Table 7, the repeatability and reproducibility of the results are generally satisfactory at 0.329-2.630 µg/mL.

3.3.3. Method of Validation

TThe inter- and intra- day precision was studied upon carrying out five determinations of MPV with three different concentrations (6.59, 13.17, and 32.93 µg/mL). By analyzing the precision parameter, we found SD and RSD% to be less than 2%, demonstrating good repeatability and intermediate precision. Furthermore, the MPV absorbance values were used to assess the between-analyst precision. The latter procedure used two analysts comparing the absorbance results to the RSD% using five replicates. According to this investigation, exceptional precision is less than 1.29%.

To assess the robustness of the proposed methods, little changes were made to the volume of the sample and wavelength. [30, 33]. As demonstrated by the precision values expressed as RSD%; 0.17-1.02, those changes have no significant impact on the results.

Two analysts were used to examine the ruggedness, and furthermore, a single analyst carried out the measurement step utilizing three different measurement cells. The data of RSD% was found to be 0.58-0.97%.

Identifying or quantifying the substance of interest is determined by its selectivity, even if other compounds are present in the sample [34]. Recoveries for added concentrations were performed to evaluate the selectivity of the proposed tool. The percentage recovery was 96.5-103.4 percent, with an average of 98.7%. The results obtained from using dosage forms containing excipients were the same as those obtained from using the pure form, showing that none of the commonly used excipients interfered with MPV determination.

The accuracy was tested by using five replicates of different concentrations (within the calibration curve limits under the given conditions) of MPV raw material. The mean percent recovery was determined to be between 97.91 and 101.96 %, indicating high accuracy and selectivity.

Table 7: Standard addition method for quantifying MPV solution in raw materials

Taken concentration	240 nm		285 nm	
µg/mL	% Recovery*	%RSD	% Recovery*	%RSD
2.630	99.29±0.36	0.36	100.62±0.44	0.44
0.988	100.35±0.64	0.64	99.98±0.14	0.14
0.659	101.15±1.02	1.01	100.53±0.24	0.24
0.329	101.92±0.91	0.89	98.54±0.16	0.16
0.165	101.31±0.94	0.93	104.56±0.11	0.11

*: Recovery ± standard deviation of five replicate measurements.

The proposed methods' accuracy may be proven by contrasting them with the HPLC method that was previously published [11]. The results of the suggested approaches were in strong agreement with the one that had previously been published.

3.3.4. Applications

These results demonstrate the suitability of the proposed methods for MPV quantification in pure forms. To study the applicability of the mini-scale methodology; MPV was measured in Molnupiravir® capsules, spiked human plasma, and urine samples where a previously published method achieved by HPLC was used as a comparison [11].

In the experimental section, the comprehensive methodologies for MPV assurance in pharmaceutical capsules were presented. The regression equation was used to calculate the drug concentration in the prepared solutions. Table 8 shows various Molnupiravir ® concentrations. The calibration curve method was used to conduct recovery experiments. The latter is in the 99.19-101.85% range, with an RSD of 0.21-1.15%, Table 8. As a result of the above data the current study can be used as aa easy, precise, and economic tool for analysis of Molnupiravir capsules® free from interferences.

Table 8: Estimation of the suggested method's precission using MPV's pharmaceuticals, urine, and spiked human serum samples

Concentration	240 nm				285 nm			
µg/mL	Recovery%*	RSD%	t-test	F-test	Recovery%*.	RSD%	t-test	F-test
				Raw material				
15.44	100.78±0.54	0.54	0.19	6.02	99.52±0.76	0.76	0.15	0.33
23.16	99.19±0.32	0.32	0.27	2.56	101.85±0.21	0.21	1.57	0.21
30.88	101.33±0.46	0.45	1.64	0.12	100.51±0.66	1.15	0.26	1.27
				MPV® (500 mg MPV/capsule)				
19.21	98.98±0.95	1.67	1.44	0.63	101.51±0.66	1.12	0.60	1.31
28.81	100.38±0.63	1.08	0.27	1.44	99.91±0.62	1.06	1.19	1.51
38.41	100.82±1.03	1.77	0.04	1.61	100.80±0.63	1.08	0.03	1.46
				Spiked human serum				
15.44	101.18±0.59	1.02	0.03	1.63	101.85±0.72	1.23	0.85	1.09
19.21	102.25±0.72	1.21	1.89	1.09	102.06±0.57	0.97	1.15	1.72
				Spiked human urine				
19.21	99.70±0.65	1.13	1.85	1.35	99.99±1.10	1.91	0.54	2.13
23.16	100.74±0.74	0.74	0.01	3.08	100.81±0.69	1.20	0.21	2.54

t-tabulated 2.78 at 95% confidence limit F- tabulated 3.179

3.3.5. Statistical Treatment

To verify the current study, a statistical comparison with another previously published tool (HPLC[11]) was carried out. The accuracy was measured by calculating the t-test while the precision was done by F test, Table 8. The tabulated values are 2.78 and 3.179 for t- and F-tests, respectively [36] at a 95% confidence limit. Table 8 shows that the obtained values are lower than the tabulated ones proving the method's precision and accuracy.

Moreover, one way ANOVA test was used to demonstrate the difference between the measured recoveries [37]. It was found from One way ANOVA's results that, As $F_{cal.}$ is less than $F_{tab.}$, Table

9 shows that there is no difference in the achieved recoveries of the various concentrations.

Table 9: One-way ANOVA of the recovery values

Variation source	Some of squares	df	Mean squares	F calculated	Sig.
Between concentration	0.9	1	0.9		
Within groups	4.0	8	0.5	1.8	0.217
Total	4.9	9			

4. Conclusions

Molnupiravir (MPV) was examined in raw materials, pharmaceutical formulations, and biological fluids using a green, accurate, linear, and cost-effective spectrophotometric approach. Theoretical spectroscopic analysis of MPV molecule was determined utilizing quantum chemical simulations with DFT. Additionally, using DFT B3LYP/6-311G** level, a geometrical study for the medication was computed, which supports the experimental findings. Utilizing various experimental spectroscopic methods, including FTIR, 1HNMR, and mass spectrometric analysis, the structural research of the medication was completed. Based on UV analysis at two wavelengths, 240 and 285 nm, the analyte was identified. The only solvent employed in this investigation was double-distilled water, making it considered green. Up to 35.0 µg/mL may be measured linearly with a r^2 of 0.997. The values for recovery are in the range 96.5 to 103.4%. Statistical calculations of the obtained data were carried out using F-test, t-test, and one way ANOVA test.

5. Conflicts of interest

The authors affirm that they have no known financial or interpersonal conflicts that might have looked to have influenced the research presented in this study.

6. References

[1] Lee C-C, Hsieh C-C, Ko W-C (2021) Molnupiravir-A Novel Oral Anti-SARS-CoV-2 Agent. Antibiotics 10:1294. https://doi.org/10.3390/antibiotics10111294

[2] Agostini ML, Pruijssers AJ, Chappell JD, Gribble J, Lu X, Andres EL, Bluemling GR, Lockwood MA, Sheahan TP, Sims AC, Natchus MG, Saindane M, Kolykhalov AA, Painter GR, Baric RS, Denison MR (2019) Small-molecule antiviral β-d-N (4)-hydroxycytidine inhibits a proofreading-intact coronavirus with a high genetic barrier to resistance. J Virol 93:. https://doi.org/10.1128/JVI.01348-19

[3] Twu S-J, Chen T-J, Chen C-J, Olsen SJ, Lee L-T, Fisk T, Hsu K-H, Chang S-C, Chen K-T, Chiang I-H, Wu Y-C, Wu J-S, Dowell SF (2003) Control Measures for Severe Acute Respiratory Syndrome (SARS) in Taiwan. Emerg Infect Dis 9:718–720. https://doi.org/10.3201/eid0906.030283

[4] Lai C-C, Shih T-P, Ko W-C, Tang H-J, Hsueh P-R (2020) Severe acute respiratory syndrome coronavirus 2 (SARS-CoV-2) and coronavirus disease-2019 (COVID-19): The epidemic and the challenges. Int J Antimicrob Agents 55:105924. https://doi.org/10.1016/j.ijantimicag.2020.105924

[5] Jamrozik E, Selgelid MJ (2020) COVID-19 human challenge studies: ethical issues. Lancet Infect Dis 20:e198–e203. https://doi.org/10.1016/S1473-3099(20)30438-2

[6] Shannon A, Selisko B, Le N-T-T, Huchting J, Touret F, Piorkowski G, Fattorini V, Ferron F, Decroly E, Meier C, Coutard B, Peersen O, Canard B (2020) Rapid incorporation of Favipiravir by the fast and permissive viral RNA polymerase complex results in SARS-CoV-2 lethal mutagenesis. Nat Commun 11:4682. https://doi.org/10.1038/s41467-020-18463-z

[7] Beigel JH, Tomashek KM, Dodd LE, Mehta AK, Zingman BS, Kalil AC, Hohmann E, Chu HY, Luetkemeyer A, Kline S, Lopez de Castilla D, Finberg RW, Dierberg K, Tapson V, Hsieh L, Patterson TF, Paredes R, Sweeney DA, Short WR, Touloumi G, Lye DC, Ohmagari N, Oh M, Ruiz-Palacios GM, Benfield T, Fätkenheuer G, Kortepeter MG, Atmar RL, Creech CB, Lundgren J, Babiker AG, Pett S, Neaton JD, Burgess TH, Bonnett T, Green M, Makowski M, Osinusi A, Nayak S, Lane HC (2020) Remdesivir for the Treatment of Covid-19 — Final Report. New England Journal of Medicine 383:1813–1826. https://doi.org/10.1056/NEJMoa2007764

[8] Vicenti I, Zazzi M, Saladini F (2021) SARS-CoV-2 RNA-dependent RNA polymerase as a therapeutic target for COVID-19. Expert Opin Ther Pat 31:325–337. https://doi.org/10.1080/13543776.2021.1880568

[9] Parsons TL, Kryszak LA, Marzinke MA (2021) Development and validation of assays for the quantification of β-D-N4-hydroxycytidine in human plasma and β-D-

N4-hydroxycytidine-triphosphate in peripheral blood mononuclear cell lysates. Journal of Chromatography B 1182:122921. https://doi.org/10.1016/j.jchromb.2021.122921

[10] Amara A, Penchala SD, Else L, Hale C, FitzGerald R, Walker L, Lyons R, Fletcher T, Khoo S (2021) The development and validation of a novel LC-MS/MS method for the simultaneous quantification of Molnupiravir and its metabolite ß-d-N4-hydroxycytidine in human plasma and saliva. J Pharm Biomed Anal 206:114356. https://doi.org/10.1016/j.jpba.2021.114356

[11] Reçber T, Timur SS, Erdoğan Kablan S, Yalçın F, Karabulut TC, Neslihan Gürsoy R, Eroğlu H, Kır S, Nemutlu E (2022) A stability indicating RP-HPLC method for determination of the COVID-19 drug molnupiravir applied using nanoformulations in permeability studies. J Pharm Biomed Anal 214:114693. https://doi.org/10.1016/j.jpba.2022.114693

[12] Frisch A (1996) Gaussian 09W Reference

[13] Becke AD (1993) Density-functional thermochemistry. III. The role of exact exchange. J Chem Phys 98:5648–5652. https://doi.org/10.1063/1.464913

[14] Lee C, Yang W, Parr RG (1988) Development of the Colle-Salvetti correlation-energy formula into a functional of the electron density. Phys Rev B 37:785–789. https://doi.org/10.1103/PhysRevB.37.785

[15] Frisch MJ, Pople JA, Binkley JS (1984) Self-consistent molecular orbital methods 25. Supplementary functions for Gaussian basis sets. J Chem Phys 80:3265–3269. https://doi.org/10.1063/1.447079

[16] Frisch A, Hratchian HP, Dennington RD, Keith TA, Millam J, Nielsen AB, Holder AJ, Hiscocks J GaussView 5 Reference

[17] El-Ghamaz NA, Diab MA, El-Bindary AA, El-Sonbati AZ, Seyam HA (2014) Geometrical structure and optical properties of antipyrine Schiff base derivatives. Mater Sci Semicond Process 27:521–531. https://doi.org/10.1016/j.mssp.2014.07.022

[18] El-Sonbati AZ, Diab MA, El-Bindary AA, Morgan ShM (2014) Supramolecular spectroscopic and thermal studies of azodye complexes. Spectrochim Acta A Mol Biomol Spectrosc 127:310–328. https://doi.org/10.1016/j.saa.2014.02.037

[19] Choudhary N, Bee S, Gupta A, Tandon P (2013) Comparative vibrational spectroscopic studies, HOMO–LUMO and NBO analysis of N-(phenyl)-2,2-dichloroacetamide, N-(2-chloro phenyl)-2,2-dichloroacetamide and N-(4-chloro phenyl)-2,2-dichloroacetamide based on density functional theory. Comput Theor Chem 1016:8–21. https://doi.org/10.1016/j.comptc.2013.04.008

[20] Painter GR, Bowen RA, Bluemling GR, DeBergh J, Edpuganti V, Gruddanti PR, Guthrie DB, Hager M, Kuiper DL, Lockwood MA, Mitchell DG, Natchus MG, Sticher ZM, Kolykhalov AA (2019) The prophylactic and therapeutic activity of a broadly active ribonucleoside analog in a murine model of intranasal venezuelan equine encephalitis virus infection. Antiviral Res 171:104597. https://doi.org/10.1016/j.antiviral.2019.104597

[21] Singh AK, Singh A, Singh R, Misra A (2021) Molnupiravir in COVID-19: A systematic review of literature. Diabetes & Metabolic Syndrome: Clinical Research & Reviews 15:102329. https://doi.org/10.1016/j.dsx.2021.102329

[22] Gao Y, Yan L, Huang Y, Liu F, Zhao Y, Cao L, Wang T, Sun Q, Ming Z, Zhang L, Ge J, Zheng L, Zhang Y, Wang H, Zhu Y, Zhu C, Hu T, Hua T, Zhang B, Yang X, Li J, Yang H, Liu Z, Xu W, Guddat LW, Wang Q, Lou Z, Rao Z (2020) Structure of the RNA-dependent RNA polymerase from COVID-19 virus. Science (1979) 368:779–782. https://doi.org/10.1126/science.abb7498

[23] Stuyver LJ, Whitaker T, McBrayer TR, Hernandez-Santiago BI, Lostia S, Tharnish PM, Ramesh M, Chu CK, Jordan R, Shi J, Rachakonda S, Watanabe KA, Otto MJ, Schinazi RF (2003) Ribonucleoside Analogue That Blocks Replication of Bovine Viral Diarrhea and Hepatitis C Viruses in Culture. Antimicrob Agents Chemother 47:244–254. https://doi.org/10.1128/AAC.47.1.244-254.2003

[24] Scrocco E, Tomasi J (1978) Electronic Molecular Structure, Reactivity and Intermolecular Forces: An Euristic Interpretation by Means of Electrostatic Molecular Potentials. pp 115–193

[25] Politzer P, Murray JS (2002) The fundamental nature and role of the electrostatic potential in atoms and molecules. Theoretical Chemistry Accounts: Theory, Computation, and Modeling (Theoretica Chimica Acta)

108:134–142. https://doi.org/10.1007/s00214-002-0363-9

[26] Sajan D, Joseph L, Vijayan N, Karabacak M (2011) Natural bond orbital analysis, electronic structure, non-linear properties and vibrational spectral analysis of l-histidinium bromide monohydrate: A density functional theory. Spectrochim Acta A Mol Biomol Spectrosc 81:85–98. https://doi.org/10.1016/j.saa.2011.05.052

[27] Lin YY, Rajesh NP, Santhana Raghavan P, Ramasamy P, Huang YC (2002) Crystal growth of two-component new novel organic NLO crystals. Mater Lett 56:1074–1077. https://doi.org/10.1016/S0167-577X(02)00680-8

[28] Issa YM, Abdel-Latif SA, El-Ansary AL, Hassib HB (2021) The synthesis, spectroscopic characterization, DFT/TD-DFT/PCM calculations of the molecular structure and NBO of the novel charge-transfer complexes of pyrazine Schiff base derivatives with aromatic nitro compounds. New Journal of Chemistry 45:1482–1499. https://doi.org/10.1039/D0NJ05397J

[29] Mohamed SH, Magdy AI, Ahmed AA (2018) Exploring the nature of the clopidogrel–bromocresol green interaction *via* spectrophotometric measurements and quantum chemical calculations. RSC Adv 8:29104–29114. https://doi.org/10.1039/C8RA05187A

[30] (2021) An Eco-Concerned Development of a Fast, Precise and Economical Spectrophotometric Assay for the Antiviral Drug Simeprevir based on Ion-Pair Formation. Biointerface Res Appl Chem 11:13474–13489. https://doi.org/10.33263/BRIAC115.134743489

[31] Monakhova YB, Kohl-Himmelseher M, Kuballa T, Lachenmeier DW (2014) Determination of the purity of pharmaceutical reference materials by ^{1}H NMR using the standardless PULCON methodology. J Pharm Biomed Anal 100:381–386. https://doi.org/10.1016/j.jpba.2014.08.024

[32] Bhattacharya S, Banerjee M (2004) Spectrophotometric and thermodynamic studies of complexation of [60]fullerene with a series of anisoles: a rational approach towards charge transfer interaction. Chem Phys Lett 396:377–383. https://doi.org/10.1016/j.cplett.2004.08.062

[33] International conference on harmonisation of technical requirements for registration of pharmaceuticals for human use ICH harmonised tripartite guideline validation of analytical procedures: text and methodology Q2(R1)

[34] Spagnol CM, Martins CJ, Kogawa AC, Isaac VLB, Salgado HRN, Corrêa MA (2022) New, Fast, and Sustainable Method by HPLC for Simultaneous Determination of Ascorbic Acid and Nicotinamide in the Study of Cosmetic Emulsions. Curr Chromatogr 9:. https://doi.org/10.2174/2213240609666220321095729

[35] J.C. Miller, J.N. Miller (1993) Statistics for Analytical Chemistry, 3rd ed. Ellis Harwood, New York, USA

[36] Hamad AE, Mohammed BS, Derayea SM, El-Malla SF (2020) Micelle sensitized synchronous spectrofluorimetric approaches for the simultaneous determination of simeprevir and ledipasvir: Application to pharmaceutical formulations and human plasma. Spectrochim Acta A Mol Biomol Spectrosc 239:118471. https://doi.org/10.1016/j.saa.2020.118471

[37] Motta C, Kogawa A, Chorilli M, Salgado H (2019) Eco-friendly and miniaturized analytical method for quantification of Rifaximin in tablets. Drug Analytical Research 3:23–29. https://doi.org/10.22456/2527-2616.98376